Research

Author for correspondence:
Michael B. Mayhew
e-mail: mayhew5@llnl.gov

THE ROYAL SOCIETY
PUBLISHING

Characterization of dependencies between growth and division in budding yeast

Michael B. Mayhew[1,2], Edwin S. Iversen[2,3] and Alexander J. Hartemink[2,3,4,5]

[1]Computational Engineering Division, Lawrence Livermore National Laboratory, Livermore, CA, USA
[2]Program in Computational Biology and Bioinformatics, [3]Department of Statistical Science, [4]Department of Computer Science, and [5]Department of Biology, Duke University, Durham, NC, USA

MBM, 0000-0001-9029-7220

Cell growth and division are processes vital to the proliferation and development of life. Coordination between these two processes has been recognized for decades in a variety of organisms. In the budding yeast *Saccharomyces cerevisiae*, this coordination or 'size control' appears as an inverse correlation between cell size and the rate of cell-cycle progression, routinely observed in G_1 prior to cell division commitment. Beyond this point, cells are presumed to complete $S/G_2/M$ at similar rates and in a size-independent manner. As such, studies of dependence between growth and division have focused on G_1. Moreover, in unicellular organisms, coordination between growth and division has commonly been analysed *within* the cycle of a single cell without accounting for correlations in growth and division characteristics *between* cycles of related cells. In a comprehensive analysis of three published time-lapse microscopy datasets, we analyse both intra- and inter-cycle dependencies between growth and division, revisiting assumptions about the coordination between these two processes. Interestingly, we find evidence (i) that $S/G_2/M$ durations are systematically longer in daughters than in mothers, (ii) of dependencies between $S/G_2/M$ and size at budding that echo the classical G_1 dependencies, and (iii) in contrast with recent bacterial studies, of negative dependencies between size at birth and size accumulated during the cell cycle. In addition, we develop a novel hierarchical model to uncover inter-cycle dependencies, and we find evidence for such dependencies in cells growing in sugar-poor environments. Our analysis highlights the need for experimentalists and modellers to account for new sources of cell-to-cell variation in growth and division, and our model provides a formal statistical framework for the continued study of dependencies between biological processes.

1. Introduction

Cell division and cell growth are processes fundamental to all life, and their dysregulation is common in diseases like cancer. In the budding yeast *Saccharomyces cerevisiae*, cell division is known to be coordinated with cell growth [1–6] (reviewed in [7]). This dependence between growth and division is most noticeable in daughter cells that, owing to the asymmetric manner of budding yeast division, are born smaller than their mothers (figure 1). Consequently, daughters undergo longer G_1 phases to reach a 'critical size' at START, the point of cell-cycle commitment [8,9]. Generally, a correlation has been observed between the birth mass of a cell and its time spent in G_1, with smaller cells at birth taking longer to complete G_1. This 'size control' is important for the maintenance of a consistent size distribution in the cell population from generation to generation (size homeostasis).

Studies of coordination between growth and division in budding yeast have focused primarily on G_1. Indeed, after having reached a sufficient and roughly similar size, both mother and daughter cells are presumed to proceed through the S, G_2 and M phases at similar rates [9,10]. These tenets of the traditional model of size control in budding yeast set certain expectations for $S/G_2/M$ duration: (i) G_1 duration is size-dependent, while $S/G_2/M$ duration is
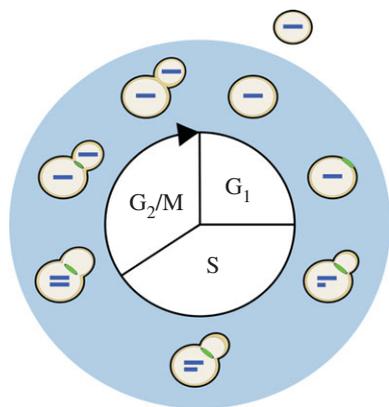
Figure 1. A diagram of the haploid budding yeast cell cycle. The process of cell division begins at the top of the diagram and proceeds clockwise. Cell division consists of G_1, S, G_2 and M; in yeast, the latter two are conceptually merged since classical studies demonstrate that they largely overlap. Along the outer ring of the diagram are depicted progressive stages of division, as reflected by the different markers of cell-cycle progression. Each bar inside the cell represents a single copy of the genome. The feature at the neck joining the mother and daughter cell represents the myosin ring. The myosin ring appears late in G_1, marking the location where the bud will emerge, and disappears with cytokinesis, indicating the separation of the mother and daughter cytoplasms. After cell wall separation, the mother and daughter cells are free to undergo more rounds of division. In budding yeast, division is asymmetric and daughters (shown outside) are born smaller than their mothers.

size-independent and (ii) $S/G_2/M$ duration is roughly constant from cell to cell. Assuming a consistent single-cell growth rate across cells, these tenets are sufficient to maintain a consistent size distribution in the population. Recent studies in bacteria have revealed an alternative size control model by which cells add a relatively constant amount of volume over the cell cycle, regardless of their birth size [11–13]. Here we use time-lapse microscopy datasets tracking characteristics of individual cells to test these models and further characterize coordination between growth and division in budding yeast.

These time-lapse datasets also allow investigation of correlations *between* measurements made at different cell cycles, an important gap in our understanding of coordination between growth and division. In multicellular systems, coordination of division among cells has important implications for higher-scale phenomena like development, differentiation and tissue organization [14–18]. In unicellular organisms like the budding yeast *S. cerevisiae*, inter-cycle dependencies between growth and division are also plausible [19] and might affect more classically studied intra-cycle dependencies or characteristics. For example, a mother cell with some advantage in cell division or growth might transmit that advantage to her progeny, resulting in a fast-dividing or fast-growing daughter cell. However, it is unclear the extent to which cell-cycle progression is correlated across cell cycles in budding yeast, if at all.

Statistical modelling provides a powerful and principled foundation for characterizing these correlations in lineages of proliferating cells. Indeed, correlation and biological lineage analysis have been intertwined at least as far back as the development of the correlation coefficient by Galton, Pearson and co-workers [14,19–23]. Statistical models of correlation in cellular characteristics have been successfully applied to bacterial and mammalian cell lineage data [24,25]. In addition, modern Bayesian inference techniques for regression and model averaging provide a framework for evaluating the plausibility of a variety of different models of correlation between growth and division [26].

Here, we provide in-depth statistical analysis to address four main biological questions: (i) Is $S/G_2/M$ duration approximately constant across cells or does it vary between mothers and daughters? (ii) Is $S/G_2/M$ duration independent of cell size? (iii) Is size at birth independent of size accumulated over the cell cycle? (iv) Is there evidence for inter-cycle dependencies in cell-cycle progression that accompany known intra-cycle dependencies? We analyse three microscopy datasets comprising different genetic and nutrient environment conditions [2]. We conduct a Bayesian regression analysis to investigate the dependence between cell growth and division within and between cycles, and comprehensively evaluate the plausibility of different models of correlation. We introduce a novel hierarchical statistical model [27,28] of budding yeast cell division at the single-cell level to formally characterize inter-cycle correlations in cell-cycle progression. Our analysis offers fresh biological and methodological insights on the extent and nature of coordination between cell division and cell growth, as well as a novel framework for formally characterizing dependencies within and between cells in these and other biological processes.

2. Single-cell analysis of size control models in budding yeast

2.1. Single-cell measurements of *Saccharomyces cerevisiae* growth and division

Single-cell data of haploid budding yeast were acquired from a previously published study [2]. The study followed cell-cycle progression and growth in 26 wild-type lineages (782 cells) grown in glucose, 19 $6 \times$ CLN3 lineages (376 cells) grown in glucose and 21 wild-type lineages (518 cells) grown in glycerol/ethanol (example lineage in figure 2). Only those cells (or a subset thereof where specified) with fully observed cell-cycle durations were retained for subsequent processing and analysis, resulting in 213 wild-type cells in glucose, 99 $6 \times$ CLN3 cells and 157 wild-type cells in glycerol/ethanol.

Cell-cycle progression was measured using the times of occurrence of two landmark cell-cycle events for each yeast cell on the plate: the appearance and disappearance of the myosin ring, visualized by tagging Myo1p with green fluorescent protein (GFP) (figures 1 and 2). The myosin ring is a contractile structure that appears late in G_1, just prior to the appearance of the bud [29] (figure 1). Cell growth was monitored with the red fluorescent protein, DsRed, which was placed under the control of the promoter of ACT1, the constitutively expressed actin gene. In this way, total red fluorescence in a cell served as a proxy for total protein content or cell mass. Red fluorescence in a cell was quantified at each time point and suitably normalized across all cells in a microcolony (electronic supplementary material, §1).

2.2. Size-dependent differences in $S/G_2/M$ duration between mothers and daughters

Budding yeast cells born at a smaller than average size tend to undergo longer G_1 phases to reach a sufficient size for cell-cycle entry, manifesting as a dependence between cell
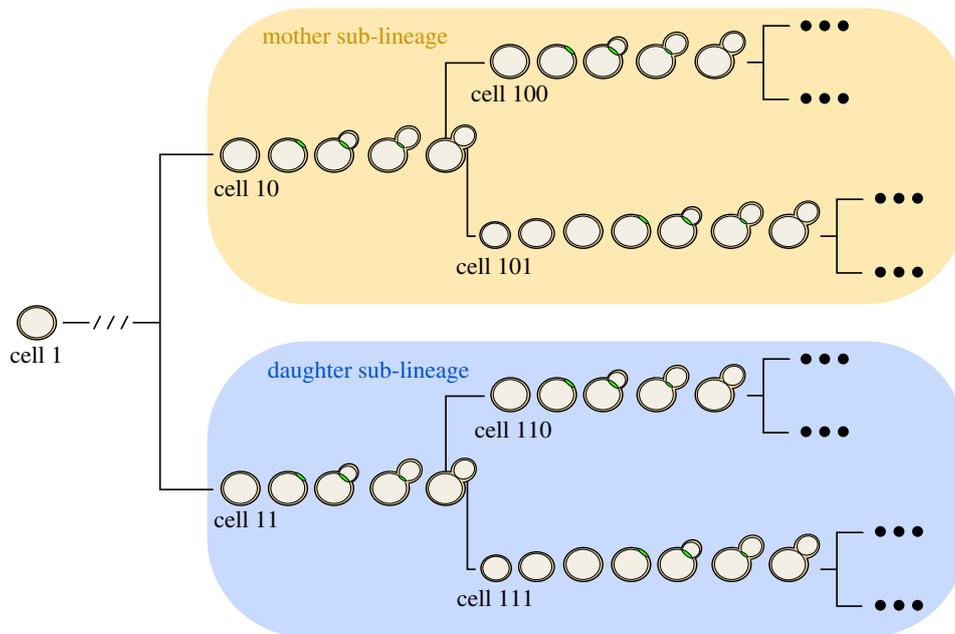
Figure 2. Illustration of single-cell lineages and classification of cell types. Shown is a typical single-cell lineage tree from the dataset of Di Talia et al. [2]. Arranged along each branch of the lineage tree are images of representative cells undergoing cell-cycle events. Binary cell labels ending in 0 indicate a mother cycle while those ending in 1 indicate a daughter cycle.
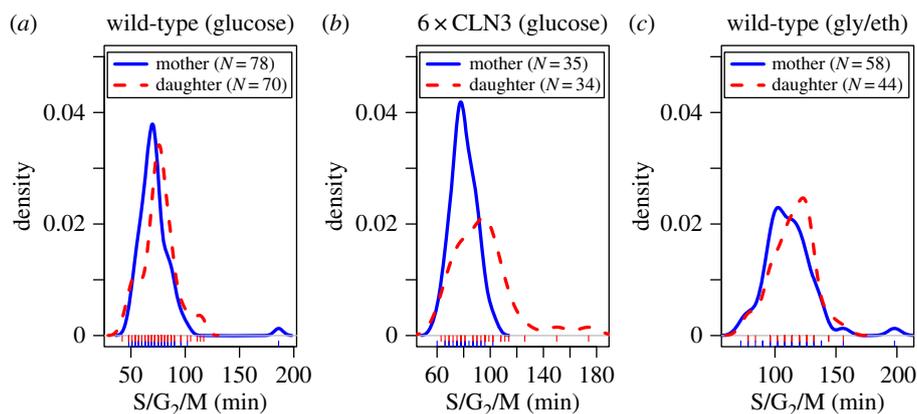

Figure 3. (a−c) Density plots of S/G_2/M durations for mother and daughter cells in the three different experimental conditions. Rug plots appear below each density plot.

size and division within a given cell cycle. Under the assumption that mothers and daughters complete G_1 at roughly the same size, the cells maintain a consistent cell size distribution from generation to generation provided the amount of time they spend in S/G_2/M is similar on average. As such, we tested whether S/G_2/M duration is similar across mother and daughter cells [9].

To assess differences in the observed mother and daughter S/G_2/M duration, we performed two-sided non-parametric Wilcoxon's rank sum tests in the three datasets (figure 3 and table 1). For this analysis, we separated mother and daughter S/G_2/M durations. We used a subset of the mother cells because some S/G_2/M durations were associated with the same mother in consecutive cell cycles (electronic supplementary material, §1). We found significantly shorter S/G_2/M durations for mothers compared with daughters for both 6 × CLN3 cells and wild-type cells growing in glucose. We also found suggestive (but not significant) differences in S/G_2/M for wild-type cells growing in glycerol/ethanol.

Table 1. Differences in S/G_2/M duration between mother and daughter cells. Cell counts are the same as in figure 3. Estimates of differences in S/G_2/M duration and 95% CIs (in parentheses) are shown.

dataset	difference (min)	p-value
wild-type (glucose)	−6 (−9, 0)	0.021
6 × CLN3	−12 (−18, −3)	0.001
wild-type (gly/eth)	−6 (−12, 0)[a]	0.166

[a]Before rounding of interval estimates for display purposes, interval for wild-type cells in glycerol/ethanol included 0 while interval for glucose did not (hence different p-values).

One potential explanation for these differences in S/G_2/M duration is that daughter cells smaller than their mothers at the onset of S/G_2/M might require more time to complete the budded period. We tested this hypothesis by pairing mother cells from the previous analysis with their first daughters. Here, mother−daughter pairs only
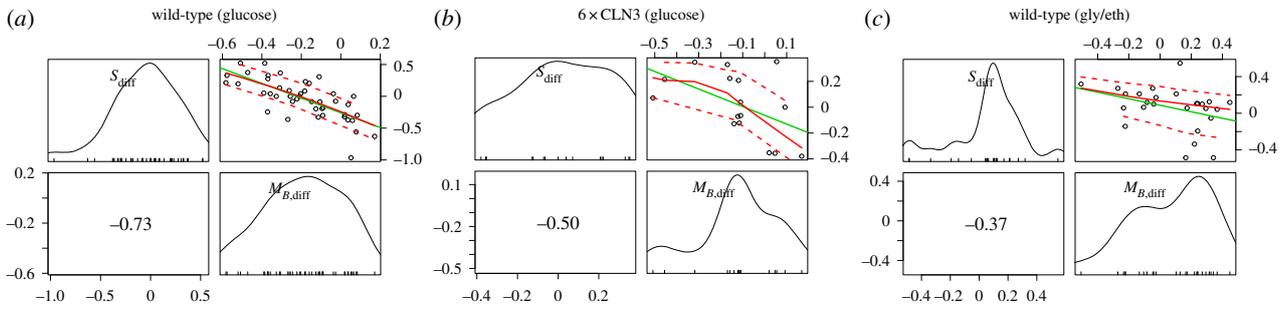
Figure 4. Scatter and marginal density plots of mother–daughter differences in log $S/G_2/M$ duration and mass at budding. Marginal density plots of each variable are shown on the diagonal. In the lower off-diagonal panels appear the Spearman's rank correlation coefficients. Scatter plots along with best linear fit lines (green), loess smoothed fit lines (solid red) and loess spread lines (dashed red; root-mean-squared positive and negative residuals) appear in the upper diagonal panels. The loess span was 1.0. Daughter–mother pair counts are those listed in table 2.

Table 2. Regression of daughter–mother differences in size at budding on differences in log $S/G_2/M$ duration. p-values (in parentheses) are for the test of zero-valued estimates. Fitted masses at budding were computed from linear regressions on the logarithm of each cell's growth traces (§2; electronic supplementary material, §2). p-values less than 0.001 are shown in scientific notation.

parameter	wild-type glucose ($N = 44$ pairs)		$6 \times$ CLN3 glucose ($N = 16$ pairs)		wild-type gly/eth ($N = 26$ pairs)	
	estimate	(p-value)	estimate	(p-value)	estimate	(p-value)
intercept	-0.26	(1.03×10^{-6})	-0.06	(0.366)	0.09	(0.068)
coefficient	-1.16	(2.19×10^{-8})	-0.68	(0.047)	-0.36	(0.061)

included daughter cells whose immediate mother was not also a daughter cell herself. We then fit a linear regression of the mother–daughter difference in log $S/G_2/M$ duration on the differences in estimated mass at budding (figure 4). In this regression model, the intercept represents the conditional expected difference between daughter and mother log $S/G_2/M$ durations independent of size differences, while the coefficient refers to the slope in terms of differences in fitted masses at budding. In two of the three experimental settings, the difference between daughter and mother mass at budding was a significant negative predictor of differences in log $S/G_2/M$ duration (table 2). Thus, daughters smaller than their mothers at the point of cell-cycle entry tend to spend more time in $S/G_2/M$. Collectively, these results provide evidence that $S/G_2/M$ duration is systematically different between mother and daughter cells, and, surprisingly, we identify a growth-related component to this difference.

2.3. Significant associations observed between size at birth and size accumulated

Recent studies in bacteria and budding yeast have suggested a compelling alternative model for size control called the 'adder' model [6,11–13] which posits that the size added by cells during the cell cycle is roughly constant from cell to cell and independent of the cell's size at birth. To evaluate evidence for this hypothesis in our data, we analysed the association between the observed birth mass (M_0) and mass accumulated between birth and division ($M_{add} = M_{div} - M_0$). Interestingly, we find strong negative correlations between mass at birth and mass accumulated over the cell's life in every cell type and every condition (figure 5).

Moreover, the correlations we observe are all significant with two-sided hypothesis tests of the Spearman's rank coefficients (table 3).

One possible explanation for the association we observe is that it is driven primarily by a negative correlation between mass at birth and size accumulated during G_1 (classical size control dependence) and that mass at birth and size accumulated during $S/G_2/M$ are uncorrelated. However, we also observe significant negative associations between mass at birth and size accumulated during $S/G_2/M$, particularly in $6 \times$ CLN3 cells (table 3). These correlations might indicate a compensatory mechanism during $S/G_2/M$ to overcome disabled G_1 size control and ensure robust cell size at division. Regardless, in aggregate, we find no evidence for 'adder' model effects in our time-lapse datasets.

2.4. Post-G_1 dependence between cell-cycle progression and cell growth

As mentioned earlier, budding yeast daughter cells tend to spend more time in G_1 than their mothers to reach a sufficient size for cell-cycle entry. This reflects an association between G_1 duration and cell size at birth. It has been hypothesized that G_1 is the primary period during which cell-cycle progression depends on cell size and that $S/G_2/M$ progression is largely independent of size, subject instead to a timing mechanism [10]. Moreover, analyses of coordination between growth and division have focused primarily on dependencies *within* rather than *across* cell cycles. However, given that budding yeast cells divide asymmetrically, leading to partitioning of organelles and other cellular contents between mothers and daughters, it is plausible that cell-cycle
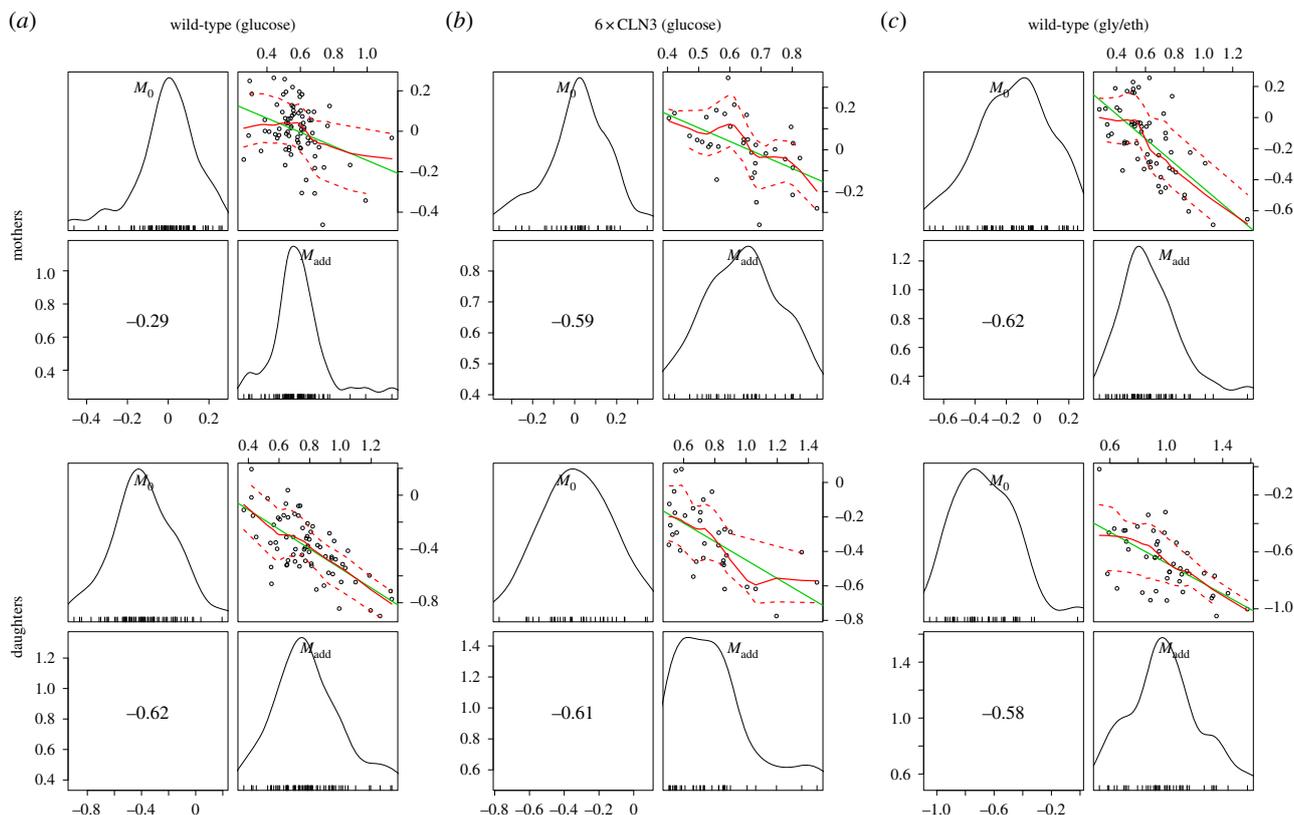
Figure 5. Scatter and marginal density plots of mass at birth and mass accumulated from birth to division for mother and daughter cells in all three experimental conditions. The layout and content of each of the six panels are the same as in figure 4. Cell counts are in table 3.

Table 3. Test of no correlation between size at birth and mass accumulated over the cell cycle. The third column shows p-values for the correlation between mass at birth (M_0) and mass added over the entire cell cycle ($M_{add, full}$). The fourth column shows p-values for the correlation between birth mass and mass added during $S/G_2/M$ ($M_{add, sg2m}$). p-values less than 0.001 are shown in scientific notation.

dataset	cell type	p-value	
		$M_{add, full}$	$M_{add, sg2m}$
wild-type	mothers ($N = 78$)	0.011	0.188
(glucose)	daughters ($N = 70$)	2.10×10^{-8}	0.183
$6 \times CLN3$	mothers ($N = 35$)	2.22×10^{-4}	0.003
	daughters ($N = 34$)	1.69×10^{-4}	0.001
wild-type	mothers ($N = 58$)	3.82×10^{-7}	0.001
(gly/eth)	daughters ($N = 44$)	4.49×10^{-5}	0.172

progression might depend on characteristics of the cell's mother as well as on the size of the cell itself.

Classically, one would analyse the correlation between a cell-cycle interval (e.g. G_1) and the cell's size at the beginning of that interval. However, by conditioning on more predictor variables, we can estimate the relative effects of a cell's size and the growth and division characteristics of its mother on the cell's current cell-cycle durations. To do this, we first computed growth characteristics of a cell and its immediate antecedent cell. Using the single-cell growth traces of each cell j and its immediate predecessor cell (Pa(j); mother cycle that immediately preceded cycle of cell j) in lineage i, we estimated

growth-related variables ($\hat{\alpha}_{i,j}$, $\hat{\alpha}_{i,Pa(j)}$, $\hat{M}_{0,i,j}$, $\hat{M}_{0,i,Pa(j)}$, $\hat{M}_{B,i,j}$ and $\hat{M}_{B,i,Pa(j)}$) by assuming exponential single-cell growth kinetics and fitting a separate linear model to the logarithm of each cell's growth trace [2] (electronic supplementary material, §2). The fitted intercept of this linear model gave the estimated birth mass ($\hat{M}_{0,i,j}$) of cell j from each lineage i while the slope gave the estimated mass accumulation rate ($\hat{\alpha}_{i,j}$). We also retained the fitted mass at budding of each cell ($\hat{M}_{B,i,j}$). We then fit linear regression models of log $S/G_2/M$ durations on these cell-level estimates as well as on the log $S/G_2/M$ durations of the cell's predecessor ($S_{i,Pa(j)}$).

Here, a model represents a particular pattern of dependence between growth and division and is determined by the set of predictor variables included in the regression. As we have seven different predictor variables (not counting the included intercept term, μ_S), there are $2^7 = 128$ possible regression models. To infer the most plausible model of dependence between size and cell-cycle progression while explicitly accounting for uncertainty in the model specification, we conducted Bayesian model averaging [26]. Since we did not have strong prior information about the dependencies between these variables, we assumed that each regression model was equally plausible a priori. We then computed posterior probabilities of each model for mother cells (figure 6) and daughter cells (figure 7). For the analysis of mothers, we retained only every other cell cycle of the mother cell starting with its most recent cycle in the lineage, to account for potential correlations between different cycles of the same mother. This procedure resulted in 53 wild-type pairs in glucose, 25 $6 \times CLN3$ pairs and 46 wild-type pairs in glycerol/ethanol. For the analysis of daughters, we used the mother–daughter pairs of our previous analysis (cell counts provided in table 2).
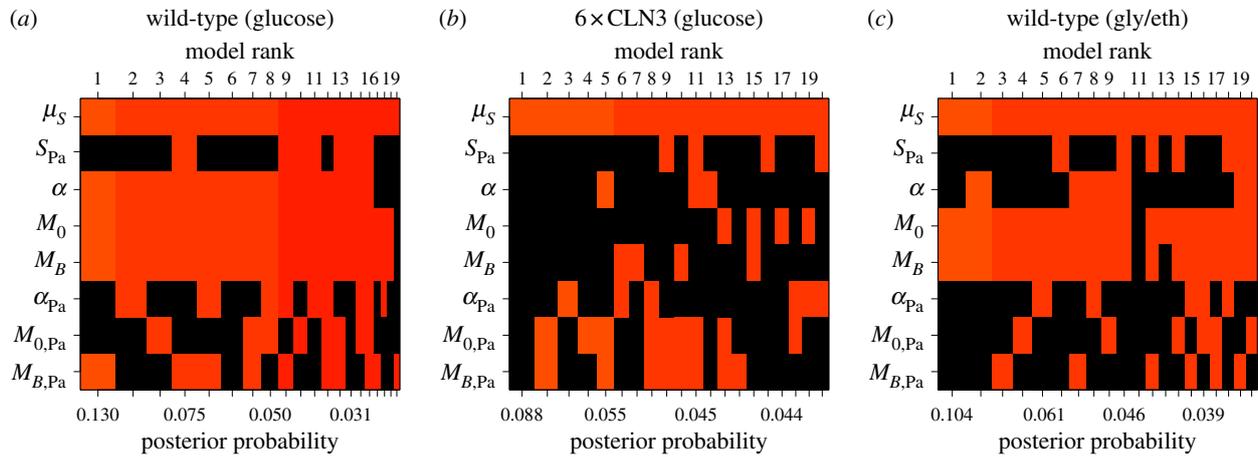
Figure 6. Bayesian adaptive sampling results for mother cells. Shown are the top 20 models (columns ranked by posterior probability) where coloured squares indicate that the corresponding predictor variable is included in the model and black squares indicate exclusion of the variable. (Online version in colour.)
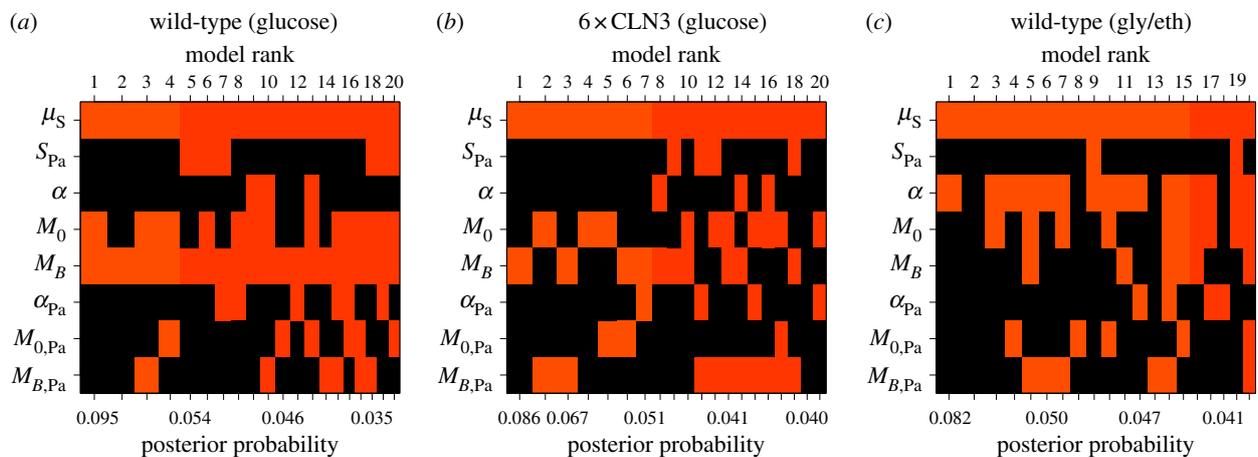

Figure 7. Bayesian adaptive sampling results for daughter cells. Panel layout and content are the same as in figure 6. (Online version in colour.)

When we consider mother-to-mother dependencies (figure 6), we find a strong association for wild-type mothers between log $S/G_2/M$ duration and growth characteristics, particularly birth mass and mass at budding. For mothers growing in glucose, mass at budding (M_B) was included in nearly every enumerated model with non-zero posterior probability, indicating that mass at budding was an informative predictor of mother log $S/G_2/M$ duration (approx. 82% posterior probability of inclusion; $\log_{10}$(Bayes factor) = 0.657 or 'substantial evidence' for inclusion [30]). Mass at birth (M_0; approx. 74% posterior probability) and mass accumulation rate (α; approx. 71% posterior probability) also tended to be included as predictors. Likewise, for a mother growing in glycerol/ethanol, we detect an association between her current log $S/G_2/M$ duration and mass at birth (approx. 64% posterior probability) and budding (approx. 61% posterior probability). In addition, the posterior means (averaged across all models) of the included regression coefficients for mass at budding for wild-type mothers in glucose (-1.129) and glycerol/ethanol (-0.262) were consistent with classical G_1 size control (larger mass at budding corresponds to less time spent in $S/G_2/M$). This pattern of dependence has not previously been observed in mother cells, potentially due to the fact that we are conditioning on multiple growth and division characteristics for the cell's current and previous cycles. We did not see such patterns of dependence for $6 \times$ CLN3

mother cells. Importantly, we also did not find strong evidence for dependence between a wild-type or $6 \times$ CLN3 mother's log $S/G_2/M$ duration and her characteristics in her previous cycle (S_{Pa}, α_{Pa}, $M_{0,Pa}$ and $M_{B,Pa}$). So, conditioned on summaries of the mother's current cycle, her log $S/G_2/M$ duration can be considered independent of her previous growth and cell-cycle progression.

Extending this analysis to mother-to-daughter associations (figure 7), we again discovered patterns of dependence between a cell's log $S/G_2/M$ duration and mass at budding (M_B) for wild-type daughter cells growing in glucose (figure 7a). Mass at budding was included as an explanatory variable for the wild-type daughter's log $S/G_2/M$ duration in glucose in nearly all models with non-zero probability (approx. 93% posterior probability of inclusion; $\log_{10}$(Bayes factor)=1.118 or 'strong evidence' for inclusion [30]). As in the previous analysis, the model-averaged posterior mean of the included regression coefficient was -0.616, an estimate consistent with classical G_1 size control. We found only mild associations between log $S/G_2/M$ duration and other growth characteristics in all three conditions (figure 7). In particular, we note an association between log $S/G_2/M$ duration and mass accumulation rate in glycerol/ethanol (α; approx. 58% posterior probability of inclusion). The model-averaged posterior mean of the included regression coefficient for mass accumulation rate was -18.391, indicating that
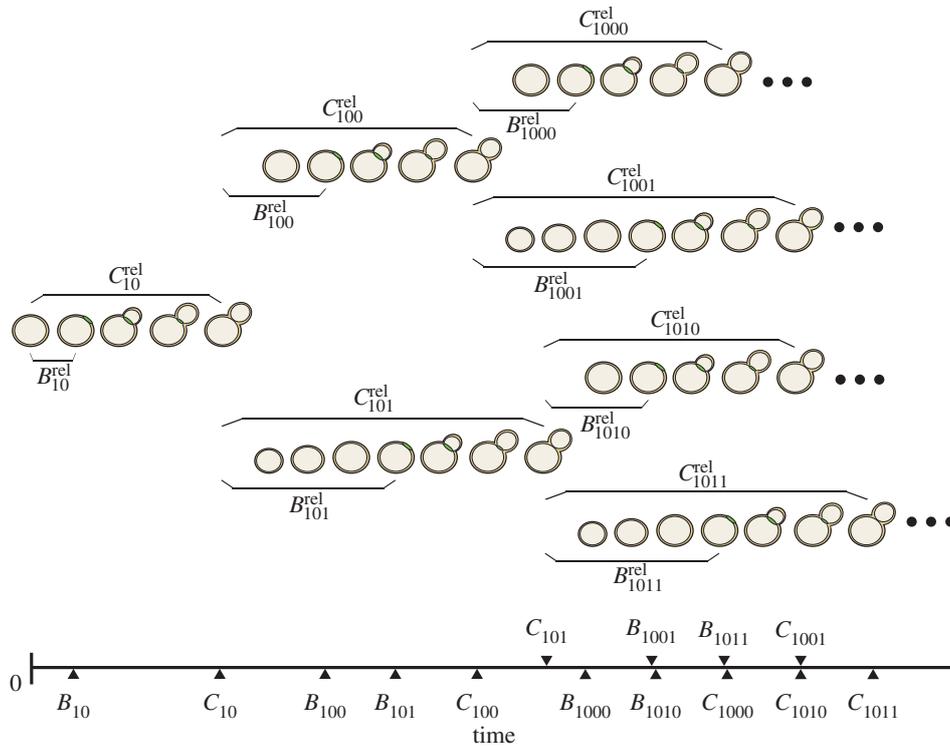
Figure 8. Sample diagram of budding and division observations arising from the time-lapse microscopy experiments. Here, an example mother origin cell (cell 10) of the sub-lineage proceeds through the cell cycle, undergoing budding and division. Dividing from her daughter (cell 101), the mother origin becomes mother cell 100 and undergoes another round of division. The ellipses following the lineage leaves indicate that lineages could be large. (Online version in colour.)

daughters with larger mass accumulation rates spend less time in $S/G_2/M$. Collectively, our findings for both mother and daughter cells run counter to the notion that $S/G_2/M$ duration is independent of size.

3. Hierarchical modelling of correlation in budding yeast cell division at the single-cell level

The regression framework used in the previous section highlighted associations between growth and division within and across cycles. However, we limited our analysis to rigidly defined mother–mother and mother–daughter pairs and did not take advantage of the inherent hierarchical organization of the data (i.e. cells make up lineages and multiple lineages are observed for each experimental condition). Moreover, simply computing sample-based estimates of inter-cell correlations would preclude separation of cell-to-cell variation in cell-cycle progression from variation due to measurement error. Hierarchical models provide a formal framework to represent such structure and naturally pool information across replicate lineages, as well as allow for estimation of cell-specific and noise-related sources of variation. An important property of these models is the potential to reduce parameter estimation error relative to sample-based approaches by 'shrinking' cell-specific parameter estimates towards sample (population) estimates [27]. For these reasons, and to more effectively characterize dependencies between cells, we developed a novel hierarchical model to analyse single-cell cell-cycle durations.

3.1. Observing a cellular branching process
To motivate our model, we consider how single-cell data are acquired using time-lapse microscopy. A single yeast

cell (the founder cell; cell 1 in figure 2) growing on the agar-ose slab is identified at the onset of the time-lapse experiment. Each founder cell generates a lineage consisting of two fully observed sub-lineages (figure 2). The mother sub-lineage consists of the founder's first cell cycle after division from its daughter (mother origin) along with all her progeny. The daughter sub-lineage consists of the founder cell's first daughter (daughter origin) and her progeny. Non-origin cells of these sub-lineages are hereafter referred to as 'mother' and 'daughter' cells.

For these sub-lineage cells, we observe the time relative to the start of the time-lapse experiment of the appearance and disappearance of the cell's myosin ring. We refer to these times as budding and division times, respectively. In our notation, the budding time for cell j from lineage i is $B_{i,j}$ and the division or cycle time is $C_{i,j}$ (figure 8). We then transform these times to cell-specific budding ($B_{i,j}^{rel}$) and division ($C_{i,j}^{rel}$) durations (figure 8; electronic supplementary material, §5.1). To refer to durations specific to each cell, we adopt the binary indexing scheme of Di Talia et al. [2].

We view the budding and division durations from each lineage (as in figure 8) as noisy observations from an underlying branching process (illustrated in figure 9). The branches of the tree in figure 9 represent the expected division durations for each cell. The cell's expected budding duration is modelled as a fraction of this branch length. To identify inter-cycle correlation in cell-cycle progression, we assume that the branch lengths in the process may depend on one another. Further details of model construction follow.

3.2. Likelihood and error model for budding and division observations
The first (lowest) level of our hierarchical model captures noise or error in observations while higher levels of the
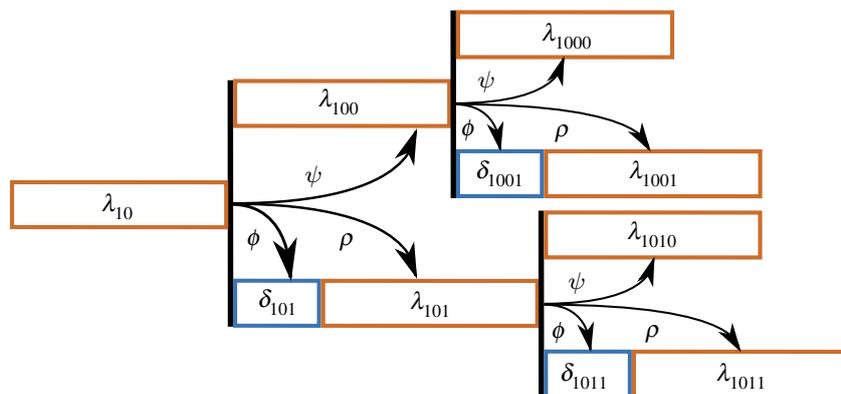
Figure 9. A diagram of the asymmetric branching process specifying expected cell-cycle durations for each cell. The diagram is drawn to indicate the branch lengths that give rise to the budding and division durations in figure 8. λ_{10} is the expected cell-cycle duration of mother origin cell 10. The expected cell-cycle duration of her subsequent cycle is λ_{100}, which depends on the length of her first cell cycle through the correlation parameter ψ. For the daughter branch, two parameters specify the cell's expected division duration: δ_{101} and λ_{101}. These branch lengths depend on the mother's cell-cycle duration through the correlation parameters ϕ and ρ, respectively. (Online version in colour.)

hierarchical model capture cell-to-cell variability. Here, we first assume that the elapsed times from which the durations for cell j in lineage i are derived are independent and normally distributed with means $\mu_{B_{i,j}}$ and $\mu_{C_{i,j}}$ and variance τ^2. While the observed cell-cycle durations are positively valued, we use normal errors at the lowest level of the hierarchical model rather than alternative error models (e.g. lognormal) because we do not expect multiplicative errors from the manual recording of budding and division events. Instead, as will be discussed in a later section, we constrain the branch length parameters to be positively valued. After transformation of elapsed times into durations, the likelihood of all budding and division durations for lineage i is

$$\begin{pmatrix} \tilde{B}_i^{\mathrm{rel}} \\ \tilde{C}_i^{\mathrm{rel}} \end{pmatrix} \bigg| \tilde{\gamma}_i, \tilde{\beta}_i, \Theta_{\mathrm{pop}}, \tau^2 \sim \mathsf{MVNorm}(A\tilde{\mu}_i, \tau^2 AA'),$$

where A is a linear transformation matrix and $\tilde{\mu}_i$ is a vector of the expected budding and division durations for lineage i. $\tilde{\gamma}_i$ is a vector containing two types of cell-specific parameters that make up the branching process of a lineage: the expected base cell-cycle durations for each cell in lineage i ($\lambda_{i,j}$s) and extensions to expected daughter cell-cycle durations due to smaller size at birth ($\delta_{i,j}$s). Θ_{pop} is the set of population-level parameters $\{\Lambda, \Delta, \sigma_\lambda^2, \sigma_\delta^2, \psi, \rho, \phi\}$ (table 4) that specify correlation and cell-to-cell variation in the $\lambda_{i,j}$s and $\delta_{i,j}$s. The vector $\tilde{\beta}_i$ contains another set of cell-specific parameters ($\beta_{i,j}$s): the fraction of cell j's λ branch spent in the unbudded phase. We describe the model for the means ($\tilde{\mu}_i$) of the observations and the remaining parameters in the next section.

3.3. Representing inter-cycle dependence and cell-to-cell variability with an asymmetric branching process

The second level of the hierarchical model consists of cell-specific parameters (e.g. branch lengths) that give the expected value of a cell's budding and division durations for a particular lineage. This second level comprises a branching process in which the branch lengths are potentially correlated and vary from cell to cell (figure 9). The branch lengths for a lineage i are represented by a vector $\tilde{\gamma}_i$, composed of two sets of parameters: $\lambda_{i,j}$s and $\delta_{i,j}$s. The δs

Table 4. Population parameters of hierarchical model.

parameter	description
Λ	population average of mother cell-cycle duration (minutes)
Δ	population average of daughter cell G_1 extension duration (minutes)
ψ	correlation between λ's from two successive mother cycles
ρ	correlation between a mother's λ and her daughter's λ
ϕ	correlation between a mother's λ and her daughter's δ
σ_λ^2	variance in cell-specific λ branch lengths (minutes^2)
σ_δ^2	variance in cell-specific δ branch lengths (minutes^2)
μ_{m}	expected proportion of λ spent unbudded in mothers
μ_{d}	expected proportion of λ spent unbudded in daughters
η_{m}	prior weight of information for mother unbudded period
η_{d}	prior weight of information for daughter unbudded period
τ^2	variance in measurement error (minutes^2)

account for longer daughter cell cycles due to smaller birth sizes. To measure correlation between these branch lengths, we introduced three parameters: ψ, ρ and ϕ (figure 9, table 4)

As noted in previous work [31,32] and since the cell-cycle durations are positively valued, we jointly model all branch lengths for a lineage i ($\tilde{\gamma}_i$) with a multivariate lognormal distribution (electronic supplementary material, §5.2). That is

$$\tilde{\gamma}_i = \exp(\tilde{\gamma}_i^*) \qquad (3.1)$$

with

$$\tilde{\gamma}_i^* \mid \Theta_{\mathrm{pop}}^* \sim \mathsf{MVNorm}(\mu_{\tilde{\gamma}_i}^*, \Sigma_{\tilde{\gamma}_i}^*). \qquad (3.2)$$

Here, $\tilde{\gamma}_i^*$ is the vector of cell-specific branch lengths on the natural logarithmic scale. These log-scale durations follow a multivariate normal distribution with a structured covariance matrix $\Sigma_{\tilde{\gamma}_i}^*$. In this covariance matrix, we encode a simple model of inter-cycle dependence. With no strong expectations of the extent of inter-cycle correlation structure, we consider the simplest model for inter-cell correlation: that the expected log-scale cell-cycle duration of a newly arisen cell depends

Table 5. Posterior inferences (modes and 95% highest posterior density intervals) for model parameters. Λ, Δ, σ_δ, σ_λ and τ are in minutes. Cell-specific unbudded duration parameters, μ_m and μ_d, range from 0 to 1.

	wild-type	6 × CLN3	wild-type
	glucose (N = 213)	glucose (N = 99)	gly/eth (N = 157)
parameter	estimate	estimate	estimate
Λ	87.60 (85.08, 90.33)	95.80 (92.40, 100.79)	145.24 (139.19, 152.34)
Δ	25.55 (20.21, 31.30)	18.57 (12.20, 23.03)	94.02 (81.68, 107.78)
μ_m	0.18 (0.16, 0.19)	0.15 (0.13, 0.17)	0.25 (0.23, 0.27)
μ_d	0.13 (0.09, 0.17)	0.05 (0.01, 0.11)	0.22 (0.17, 0.27)
η_m	23.19 (18.45, 28.77)	25.48 (19.02, 33.19)	22.84 (17.89, 28.49)
η_d	16.53 (11.51, 23.33)	20.39 (13.48, 28.22)	23.37 (16.56, 31.56)
ψ	−0.07 (−0.31, 0.20)	−0.03 (−0.38, 0.50)	0.46 (0.22, 0.65)
ρ	−0.18 (−0.41, 0.08)	−0.29 (−0.61, 0.12)	0.21 (−0.13, 0.51)
ϕ	−0.20 (−0.40, 0.05)	−0.64 (−0.84, 0.01)	−0.02 (−0.26, 0.24)
σ_δ	20.00 (14.63, 30.32)	6.56 (2.83, 10.11)	42.65 (33.16, 56.56)
σ_λ	15.30 (13.66, 17.20)	15.72 (13.49, 18.82)	26.07 (22.54, 30.11)
τ	1.31 (0.93, 1.91)	1.43 (0.99, 2.30)	1.45 (0.96, 2.30)

solely on the expected log-scale cell-cycle duration of its predecessors in the lineage only through its mother. As we do not observe the cell-cycle durations of each lineage's founder cell (figure 2), this correlation structure dictates that the branch lengths of the mother origin and daughter origin are correlated with one another, and we model them accordingly (electronic supplementary material, §6).

The mean vector $\mu_{\tilde{\gamma}_i}^*$ consists of parameters Λ^* and Δ^* (counterparts of Λ and Δ on the log scale). $\Sigma_{\tilde{\gamma}_i}^*$ is parametrized by log-scale analogues of ψ, ρ, ϕ, σ_δ and σ_λ (Θ_{pop}^*). To infer parameters on the original scale (table 4), we transform the log-scale analogues (electronic supplementary material, §5.2).

As with the λ and δ parameters, each cell has a parameter indicating the proportion of its $\lambda_{i,j}$ it spends in the unbudded state: $\beta_{i,j}$. The vector $\tilde{\beta}_i$ comprises these cell-specific parameters for lineage i.

Now, we can compute the expected value of a cell's observed budding and division durations. For example, if a cell j is a mother cell then

$$\mu_{B_{i,j}} = E[B_{i,j}^{rel} \mid \tilde{\gamma}_i, \tilde{\beta}_i, \Theta_{pop}] = \beta_{i,j}\lambda_{i,j} \qquad (3.3)$$

and

$$\mu_{C_{i,j}} = E[C_{i,j}^{rel} \mid \tilde{\gamma}_i, \tilde{\beta}_i, \Theta_{pop}] = \lambda_{i,j}. \qquad (3.4)$$

On the other hand, if cell j is a daughter cell, then

$$\mu_{B_{i,j}} = E[B_{i,j}^{rel} \mid \tilde{\gamma}_i, \tilde{\beta}_i, \Theta_{pop}] = \delta_{i,j} + \beta_{i,j}\lambda_{i,j} \qquad (3.5)$$

and

$$\mu_{C_{i,j}} = E[C_{i,j}^{rel} \mid \tilde{\gamma}_i, \tilde{\beta}_i, \Theta_{pop}] = \delta_{i,j} + \lambda_{i,j}. \qquad (3.6)$$

The third level of our hierarchical model (represented by population-level parameters Θ_{pop}; table 4) encapsulates patterns of cell-cycle progression and inter-cycle dependence shared across replicate lineages in a given experimental condition. Owing to the hierarchical structure of the data, we assume for each experimental condition that the branch

lengths ($\lambda_{i,j}$s and $\delta_{i,j}$s) from all lineages are drawn from the same distribution: the multivariate lognormal distribution parametrized by Λ, Δ and other parameters of Θ_{pop}. More formally, the branch lengths are exchangeable within a given experimental condition [27]. We make a similar assumption for the cell-specific $\beta_{i,j}$s: the unbudded proportions are exchangeable and drawn from beta distributions for a given cell type (mother or daughter) and experimental setting:

$$\beta_{i,j} \sim \begin{cases} \text{beta}(\mu_m\eta_m, (1-\mu_m)\eta_m) & \text{if cell } j \text{ is a mother} \\ \text{beta}(\mu_d\eta_d, (1-\mu_d)\eta_d) & \text{if cell } j \text{ is a daughter.} \end{cases}$$
$$(3.7)$$

3.4. Hierarchical model fitting uncovers variation in cell-cycle progression across experimental conditions and between mothers and daughters

Fits of the hierarchical model to the three different datasets suggest distinct patterns of cell-cycle progression. As shown in table 5, population average mother cell-cycle duration (Λ) was approximately 88 min for wild-type cells in glucose. By contrast, mother cells divided nearly twice as slowly in glycerol/ethanol (approx. 146 min). Since Cln3 is a rate-limiting factor for cell-cycle entry [2,33], daughters with six copies of CLN3 show quite short G_1 extensions (Δ) compared with wild-type daughters grown in glucose (table 5). Likewise, the estimated spread in 6 × CLN3 daughter G_1 extensions (σ_δ^2) was much smaller compared with the corresponding estimates for wild-type cells, reflecting greater availability of Cln3 protein [2]. By contrast, wild-type daughters in glycerol/ethanol took nearly 95 min more to complete G_1 (on average) than their mothers [34].

A benefit of our hierarchical approach is the ability to separate cell-to-cell variation in cell-cycle progression from measurement error. As mentioned previously, while inferences for σ_λ do not change much between the two types of cells grown in glucose, σ_δ is dramatically reduced in 6 ×

CLN3 cells reflecting differences in cell-cycle progression one might expect. However, since the cells were grown in similar conditions, differences in cell-cycle progression should have little effect on an experimenter's ability to record budding and division times, and so measurement error should be similar. Importantly, inferences for τ for all three conditions are similar to one another (95% CIs overlap).

As part of our deeper investigation of inter-cycle dependence, we generated inferences for the three correlation parameters in the model (ρ, ψ and ϕ). As shown in table 5, no strong correlations exist in the two strains grown in glucose (wild-type and $6 \times$ CLN3) with all 95% posterior confidence intervals overlapping 0. However, we do see moderate mother-to-mother λ correlations (ψ) for wild-type cells grown in glycerol/ethanol. Because we did not detect mother-to-daughter correlations in the same conditions, the inferences for ψ suggest that cells in glycerol/ethanol tend to retain the rate of cell-cycle progression with which they are born. This correlation could not be explained by drift in cell-cycle progression due to a cell's replicative age or time spent by the cells on the plate (electronic supplementary material, §12). However, considering our previous Bayesian regression analysis (§2.4), this cell-cycle dependence is likely mediated by growth characteristics of the mother cell in her current cycle. To rule out the possibility that this result is an artefact of over-fitting the data, we carried out a leave-one-out cross-validation analysis to evaluate the capacity of different models of inter-cycle correlation to predict the observed cell-cycle durations of left-out cells. The results of this analysis were consistent with our parameter inferences in that models lacking ψ predicted the observed cell-cycle duration of wild-type cells in glycerol/ethanol more poorly (electronic supplementary material, §11). Overall, our statistical framework has generated valuable insights into potential inter-cycle sources of variation in biological processes.

4. Discussion and conclusion

In this analysis, we set out to address questions regarding dependencies within and between the fundamental processes of growth and division. We have found evidence from our analysis contradicting (i) a relatively constant $S/G_2/M$ duration shared by mother and daughter cells and (ii) a lack of dependence between $S/G_2/M$ duration and size, two previously held tenets of yeast size control. Our statistical analysis, including inferences from our hierarchical model (electronic supplementary material, §10), also demonstrates that combined $S/G_2/M$ duration appears longer on average in daughter cells compared with mother cells. Moreover, we detect a size-related component underlying these differences in $S/G_2/M$ duration. In support of our results, at least one classical study with single cells has noted that the budded duration was mildly longer (5–8 min on average) for daughters compared with mothers under a range of different growth conditions [35]. These observations are important because experimenters and modellers might otherwise assume approximately similar $S/G_2/M$ durations across cell types or simpler dependence structure between size, G_1 and $S/G_2/M$ that might not be present in their experimental conditions, potentially affecting downstream conclusions about coordination between growth and division.

Our Bayesian regression analysis uncovered patterns of dependence between cell size characteristics and $S/G_2/M$

duration for wild-type cells in two different nutrient conditions. Post-G_1 dependence between growth and division has been observed in budding yeast strains engineered for phase locking [36] and predicted by dynamic models of cell-cycle progression [32,36]. In particular, we note phenotypic similarities between the post-G_1 size dependence we observe in $6 \times$ CLN3 cells and that observed in a study of strains in which the G_1 cyclin, CLN2, was under the control of the inducible MET3 promoter [36]. As in that study, we see both reduced G_1 duration variability (σ_δ in table 5) and overall cell-cycle durations in $6 \times$ CLN3 cells similar to wild-type cells. Our analysis more comprehensively demonstrates these patterns in $S/G_2/M$, identifying these dependencies in wild-type cells and in mother cells as well as daughter cells, on which size control studies have traditionally been focused. Our analysis also takes into account new sources of variation (e.g. inter-cell dependencies) to qualify these dependencies. This analysis, coupled with our finding of no evidence for 'adder' model effects in our data, add to evidence for compensation in cell-cycle time during $S/G_2/M$ and raises the question of whether size control might exist outside of G_1 in budding yeast.

Dual, complementary mechanisms of size control have been noted in the fission yeast, *Schizosaccharomyces pombe*, with a strong size control imposed at the G_2/M boundary and a weaker compensatory size control imposed at the G_1/S boundary [10]. In addition, cell-autonomous size sensing or compensatory modulation of growth rates during the cell cycle has been postulated in multicellular systems [18]. However, while our findings seem at first glance to extend the classical model of size control in budding yeast, we caution that this observed dependence does not necessarily imply a true size control mechanism. Rather, this association could be related to compensation in cell-cycle time due to premature cell-cycle entry or the activation of a cell-cycle checkpoint [37] due to perturbed cell-cycle progression.

Consequently, our analysis has generated experimentally testable hypotheses about the molecular basis of post-G_1 size dependence and insights for future studies of size control. While the dependence we observe in $6 \times$ CLN3 cells, for example, is likely not due to activation of the morphogenesis checkpoint [38], other molecular targets related to DNA replication checkpoints (e.g. Rad53) or cryptic budding yeast size control (e.g. Bck2) should be tested to ascertain their relative effects on dependence between mass at budding and duration of $S/G_2/M$. Recent experimental work in budding yeast suggests an intriguing mechanistic model for size control in which dilution of Whi5 as the cell grows in volume dictates cell cycle entry near the G_1/S transition [5]. Our work could be extended to analyse changes in concentration of Whi5 and other proteins during $S/G_2/M$ to identify potential mechanistic bases for the dependencies we observe.

We do not detect evidence in our datasets for an 'adder' model of size control. Instead, we detect substantial negative dependencies between size at birth and size accumulated over the cell cycle. An important distinction between the current study and previous analyses is the measurement of cell size. In our datasets, cell size was measured via a fluorescent protein-based proxy for cell mass, whereas recent work in bacteria and budding yeast has focused on cell volume [6,11–13]. Elements of cell volume in budding yeast, particularly the vacuoles, are known to undergo dynamic, regulated changes over the course of the cell

cycle [39]. On the other hand, it is unclear the extent to which the fluorescent protein construct used in Di Talia's datasets is the best proxy for cell size in the absence of direct measurements of cell mass. Therefore, further experimental and analytical studies are required to reconcile these results and determine whether the method of cell size measurement has any effect on mechanistic conclusions about size control.

In addition, we have developed a novel hierarchical model of budding yeast cell-cycle progression. In uncovering correlations in cell-cycle progression between wild-type mother cycles in glycerol/ethanol, our model highlights a common theme in multicellular organism analyses [18] as well as a potential need for considering between and within cell dependencies in unicellular organism studies. If capturing cell-to-cell dependence is an experimental goal, then time-lapse microscopy is preferable over techniques involving fixed and independent samples taken over time from an initially synchronized population of cells. From a statistical perspective, observing more lineages and more generations per lineage allows for better characterization of this dependence. Our analysis also suggests that both single-cell experimentalists and modellers should at least consider the possibility of such dependence to avoid potential confounding of other observed between-cell or within-cell dependencies. Dependence between cell growth and cell division has been thoroughly studied within a given cell cycle. However, the possibility that this correlation might be mediated by inter-cycle dependencies brought about by changes in environment or nutrient availability cannot be ignored. Correlations within a cycle could disappear or decrease in magnitude when conditioning on characteristics of the previous cell or generation. Conversely, conditioning on additional variables from previous cell cycles might not affect an observed correlation, providing greater context for experimental follow-up or model construction. In either case, our analysis demonstrates that both experimentalists and modellers can benefit from considering multi-generational data acquisition and analysis to verify the robustness of their correlation inferences.

Our model provides a flexible and extensible platform for analysis of intra-cycle as well as inter-cycle dependencies.

The hierarchical specification of our model and our Bayesian approach to inference easily accommodates new lineage information. We also note that the model is not limited to cell division observations and can be adapted to the statistical analysis of dependence in any biological process (e.g. by dropping the budding yeast-specific δ and ϕ parameters and treating the λ branch parameters as the sole quantity of interest). While we modelled the branch lengths with a lognormal distribution, other distributions exist that could improve fit to data and form the basis of future work [40]. In addition, while we made use of single-cell growth data in our regression analysis, we are finalizing development of extensions to the hierarchical model to formally fit both the growth and division measurements in a joint analysis, making for a powerful tool to estimate correlations between multiple biological processes while accounting for dependencies between cells in a lineage.

This work represents an important step towards understanding the dependencies in cell-cycle progression and cell growth within and across cells in a dividing population. The statistical model-based approaches described here—coupled with ongoing time-lapse microscopy studies—will shed new light on cell-cycle and cell growth regulation and reveal mechanistic insights about the coordination between these two fundamental biological processes.

References

1. Johnston GC, Pringle JR, Hartwell LH. 1977 Coordination of growth with cell division in the yeast Saccharomyces cerevisiae. Exp. Cell. Res. **105**, 79–98. (doi:10.1016/0014-4827(77)90154-9)

2. Di Talia S, Bean JM, Siggia ED, Cross FR. 2007 The effects of molecular noise and size control on variability in the budding yeast cell cycle. Nature **448**, 947–951. (doi:10.1038/nature06072)

3. Goranov AI, Cook M, Ricicova M, Ben-Ari G, Gonzalez C, Hansen C, Tyers M, Amon A. 2009 The rate of cell growth is governed by cell cycle stage. Genes Dev. **23**, 1408–1422. (doi:10.1101/gad.1777309)

4. Ferrezuelo F, Colomina N, Palmisano A, Gari E, Gallego C, Csikasz-Nagy A, Aldea M. 2012 The critical size is set at a single-cell level by growth rate to attain homeostasis and adaptation. Nat. Commun. **3**, 1012. (doi:10.1038/ncomms2015)

5. Schmoller KM, Turner JJ, Koivomagi M, Skotheim JM. 2015 Dilution of the cell cycle inhibitor Whi5 controls budding-yeast cell size. Nature **526**, 268–272. (doi:10.1038/nature14908)

6. Soifer I, Robert L, Amir A. 2016 Single-cell analysis of growth in budding yeast and bacteria reveals a common size regulation strategy. Curr. Biol. **26**, 356–361. (doi:10.1016/j.cub.2015.11.067)

7. Turner JJ, Ewald JC, Skotheim JM. 2012 Cell size control in yeast. Curr. Biol. **22**, R350–R359. (doi:10.1016/j.cub.2012.02.041)

8. Hartwell LH. 1974 Saccharomyces cerevisiae cell cycle. Bacteriol. Rev. **38**, 164–198.

9. Hartwell LH, Unger MW. 1977 Unequal division in Saccharomyces cerevisiae and its implications for the control of cell division. J. Cell Biol. **75**, 422–435. (doi:10.1083/jcb.75.2.422)

10. Rupes I. 2002 Checking cell size in yeast. Trends Genet. **18**, 479–485. (doi:10.1016/S0168-9525(02)02745-2)

11. Campos M, Surovtsev IV, Kato S, Paintdakhi A, Beltran B, Ebmeier SE, Jacobs-Wagner C. 2014 A constant size extension drives bacterial cell size homeostasis. Cell **159**, 1433–1446. (doi:10.1016/j.cell.2014.11.022)

12. Taheri-Araghi S, Bradde S, Sauls JT, Hill NS, Levin PA, Paulsson J, Vergassola M, Jun S. 2015 Cell-size control and homeostasis in bacteria. Curr. Biol. **25**, 385–391. (doi:10.1016/j.cub.2014.12.009)

13. Jun S, Taheri-Aghari S. 2015 Cell-size maintenance: universal strategy revealed. Trends Microbiol. **23**, 4–6. (doi:10.1016/j.tim.2014.12.001)

14. Smith JA, Martin L. 1973 Do cells cycle? *Proc. Natl Acad. Sci. USA* **70**, 1263–1267. doi:10.1073/pnas.70.4.1263

15. Neufeld TP, de la Cruz AF, Johnston LA, Edgar BA. 1998 Coordination of growth and cell division in the *Drosophila* wing. *Cell* **93**, 1183–1193. (doi:10.1016/S0092-8674(00)81462-2)

16. Hawkins ED, Markham JF, McGuinness LP, Hodgkin PD. 2009 A single-cell pedigree analysis of alternative stochastic lymphocyte fates. *Proc. Natl Acad. Sci. USA* **106**, 13 457–13 462. (doi:10.1073/pnas.0905629106)

17. Pauklin S, Vallier L. 2013 The cell-cycle state of stem cells determines cell fate propensity. *Cell* **155**, 135–147. (doi:10.1016/j.cell.2013.08.031)

18. Ginzberg MB, Kafri R, Kirschner M. 2015 On being the right (cell) size. *Science* **348**, 1245075. (doi:10.1126/science.1245075)

19. Powell EO. 1958 An outline of the pattern of bacterial generation times. *J. Gen. Microbiol.* **18**, 382–417. (doi:10.1099/00221287-18-2-382)

20. Galton F. 1894 *Natural inheritance*, 5th edn. New York, NY: MacMillan.

21. Pearson K. 1896 Mathematical contributions to the theory of evolution. III. Regression, heredity and panmixia. *Phil. Trans. R. Soc. Lond. A* **187**, 253–318. (doi:10.1098/rsta.1896.0007)

22. Stewart EJ, Madden R, Paul G, Taddei F. 2005 Aging and death in an organism that reproduces by morphologically symmetric division. *PLoS Biol.* **3**, e45. (doi:10.1371/journal.pbio.0030045)

23. Leander R, Allen EJ, Garbett SP, Tyson DR, Quaranta V. 2014 Derivation and experimental comparison of cell-division probability densities. *J. Theor. Biol.* **359**, 129–135. (doi:10.1016/j.jtbi.2014.06.004)

24. Cowan R, Staudte R. 1986 The bifurcating autoregression model in cell lineage studies. *Biometrics* **42**, 769–783. (doi:10.2307/2530692)

25. Huggins RM, Basawa IV. 1999 Extensions of the bifurcating autoregressive model for cell lineage studies. *J. Appl. Prob.* **36**, 1225–1233. (doi:10.1239/jap/1032374768)

26. Clyde MA, Ghosh J, Littman ML. 2011 Bayesian adaptive sampling for variable selection and model averaging. *J. Comput. Graph. Stat.* **20**, 80–101. (doi:10.1198/jcgs.2010.09049)

27. Greenland S. 2000 Principles of multilevel modelling. *Int. J. Epidemiol.* **29**, 158–167. (doi:10.1093/ije/29.1.158)

28. Gelman A, Carlin JB, Stern HS, Dunson DB, Vehtari A, Rubin DB. 2013 *Bayesian data analysis*, 3rd edn. Boca Raton, FL: CRC Press.

29. Bi E, Maddox P, Lew DJ, Salmon ED, McMillan JN, Yeh E, Pringle JR. 1998 Involvement of an actomyosin contractile ring in *Saccharomyces cerevisiae* cytokinesis. *J. Cell Biol.* **142**, 1301–1312. (doi:10.1083/jcb.142.5.1301)

30. Kass RE, Raftery AE. 1995 Bayes factors. *J. Am. Stat. Assoc.* **90**, 773–795. (doi:10.1080/01621459.1995.10476572)

31. Dowling MR, Kan A, Heinzel S, Zhou JHS, Marchingo JM, Wellard CJ, Markham JF, Hodgkin PD. 2014 Stretched cell cycle model for proliferating lymphocytes. *Proc. Natl Acad. Sci. USA* **111**, 6377–6382. (doi:10.1073/pnas.1322420111)

32. Oguz C, Palmisano A, Laomettachit T, Watson LT, Baumann WT, Tyson JJ. 2014 A stochastic model correctly predicts changes in budding yeast cell cycle dynamics upon periodic expression of CLN2. *PLoS ONE* **9**, e96726. (doi:10.1371/journal.pone.0096726)

33. Cross F, Blake C. 1993 The yeast Cln3 protein is an unstable activator of Cdc28. *Mol. Cell. Biol.* **13**, 3266–3271. (doi:10.1128/MCB.13.6.3266)

34. Broach JR. 2012 Nutritional control of growth and development in yeast. *Genetics* **192**, 73–105. (doi:10.1534/genetics.111.135731.)

35. Lord PG, Wheals AE. 1981 Variability in individual cell cycles of *Saccharomyces cerevisiae*. *J. Cell Sci.* **50**, 361–376.

36. Charvin G, Cross FR, Siggia ED. 2009 Forced periodic expression of G1 cyclins phase-locks the budding yeast cell cycle. *Proc. Natl Acad. Sci. USA* **106**, 6632–6637. (doi:10.1073/pnas.0809227106)

37. Sidorova JM, Breeden LL. 2002 Precocious S-phase entry in budding yeast prolongs replicative state and increases dependence upon Rad53 for viability. *Genetics* **160**, 123–136.

38. McNulty JJ, Lew DJ. 2005 Swe1p responds to cytoskeletal perturbation, not bud size, in *S. cerevisiae*. *Curr. Biol.* **15**, 2190–2198. (doi:10.1016/j.cub.2005.11.039)

39. Weisman LS. 2003 Yeast vacuole inheritance and dynamics. *Annu. Rev. Genet.* **37**, 435–460. (doi:10.1146/annurev.genet.37.050203.103207)

40. Golubev A. 2016 Applications and implications of the exponentially modified gamma distribution as a model for time variabilities related to cell proliferation and gene expression. *J. Theor. Biol.* **393**, 203–217. (doi:10.1016/j.jtbi.2015.12.027)